Study on detection of michel electrons in Super-ORCA

Bachelorarbeit aus der Physik

Vorgelegt von

Sebastian Schindler

28.07.2017

Erlangen Centre for Astroparticle Physics

Physikalisches Institut

Friedrich-Alexander-Universität Erlangen-Nürnberg

Betreuer: Dr. Thomas Eberl

Contents

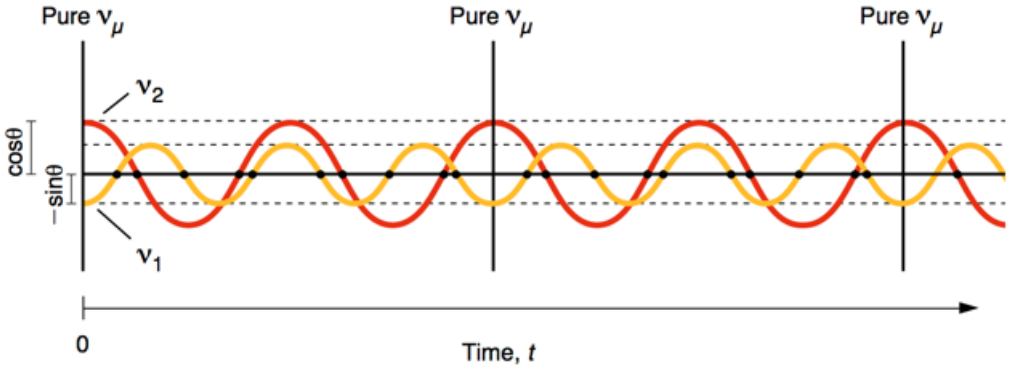

Figure 1: Simplified flavour oscillation of a muon neutrino. It is created as a "pure" muon neutrino, looses this pure state with ongoing propagation and assumes it again later due to the mass eigenstates ν_1 and ν_2 having the same phase to each other again. Taken from [3].

1 Scientific background

1.1 Neutrino oscillation

Neutrinos are weakly interacting particles that are created (and measured) as one of three flavours: Electron, muon and tau neutrino. Originally thought to be massless particles, their non-zero mass has been established as a consequence of observed flavour oscillation [2].

This is so because each flavour eigenstate does not have one corresponding mass eigenstate but is actually a superposition of all three mass eigenstates. This means that the observed flavour of a neutrino is determined by how the mass eigenstates mix. A change in proportions between the mass eigenstates can therefore result in a change of neutrino flavour. Due to the phases of the mass eigenstates being dependant on their mass a resulting phase shift changes the mixing of the mass eigenstates during propagation. Fig. 1 demonstrates the effect.

This causes the neutrino flavour to oscillate: a neutrino created with a flavour α may be measured as a neutrino with flavour β after some propagation length L. The probability for this flavour change is given as

$$P_{\alpha\to\beta} = \sum_{j,k=1}^{3} U(\alpha,\beta,j,k)\exp\left(-\frac{i}{2}\frac{L}{E}\Delta m^2_{jk}\right) \tag{1}$$

with E being the energy of the neutrino and $\Delta m^2_{jk} = m^2_j - m^2_k$ the squared-mass difference [1]. U is some product of components of the PMNS matrix, which mediates between flavour and mass eigenstates. The PMNS matrix contains various constants describing the nature of the mixing and which to measure is of great physical interest.

1.2 Current neutrino research

Experimentally the neutrino flavour oscillation is observed as a discrepancy in flux of one specific neutrino flavour compared to the flux of this flavour at the origin of the neutrinos (or nearer towards it). Being able to discriminate between neutrino flavours in a detector and knowing the ratio between the fluxes of the flavours allows to measure $P_{\alpha\to\beta}$ using statistical data. If L and E are known too, the constants in the PMNS matrix and/or the squared-mass differences can be measured.

1.2.1 Mass hierarchy

Neutrino research established only recently the mixing angles inside the PMNS matrix ([4] p. 1), leaving parameters linked to the majorana/dirac nature and possible CP violation of neutrinos

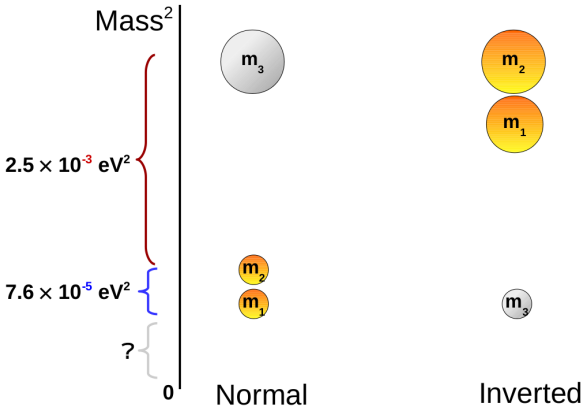

Figure 2: Neutrino mass hierarchy: normal and inverted hierarchy with squared-mass differences. The sign of the larger difference is undetermined yet. The unknown absolute masses are also indicated. Source: [5].

undetermined. Of the squared-mass differences Δm^2_{jk} only two are independent from each other with one of these being known and the others absolute value being known. Measuring the sign of the second squared-mass difference - determining the so-called neutrino mass hierarchy - is beneficial for experiments in search for the still undetermined parameters ([1] p. 32).

It is convention to start the numbering of the mass eigenstates (from 1 to 3) with the two eigenstates that have the smaller distance in mass and call the remaining eigenstate that is far away from the other two m_3. As the sign of the larger distance is unknown, two arrangements of masses are possible, called the "normal hierarchy" (numbered from 1 to 3 with increasing mass) and "inverted hierarchy" (numbered $3 \rightarrow 1 \rightarrow 2$). Fig. 2 visualizes the mass hierarchy.

Further investigation of (1) reveals that the sign of Δm^2_{jk} cannot be measured[1] for propagation in vacuum. However, propagation of the neutrinos through matter has additional effects (namely interactions between electron neutrinos and the electrons in matter) that allow for a detector to be sensitive to the sign of the squared-mass difference.

1.2.2 CP violation

Apart from solving the neutrino mass hierarchy, another fundamental physical property of neutrinos that is of interest is whether CP symmetry is violated in the weak interactions of neutrinos. A system follows parity symmetry (short: P symmetry) if it is invariant when mirrored, i.e. all physical processes are the same when reflecting the system along some plane. CP symmetry combines parity and charge conjugation symmetry, so that the spatial mirroring together with conjugating all charges leaves the system invariant.

After the Wu experiment [6] in 1956 measured violation of parity symmetry in the weak interaction CP symmetry was proposed. However, also CP symmetry is violated for (some) mesons [7], which raises the question whether CP symmetry is violated in the lepton sector too. This question can be important to research concerning leptogenesis in the very early universe.

The PMNS matrix contains a phase parameter δ_{CP}, which if non-zero is evidence for CP violation in neutrino interactions [8].

[1] One finds that it is an argument of an even function in the real part and the imaginary part does vanish if CP symmetry is not violated (which is unknown). See [1] p. 24.

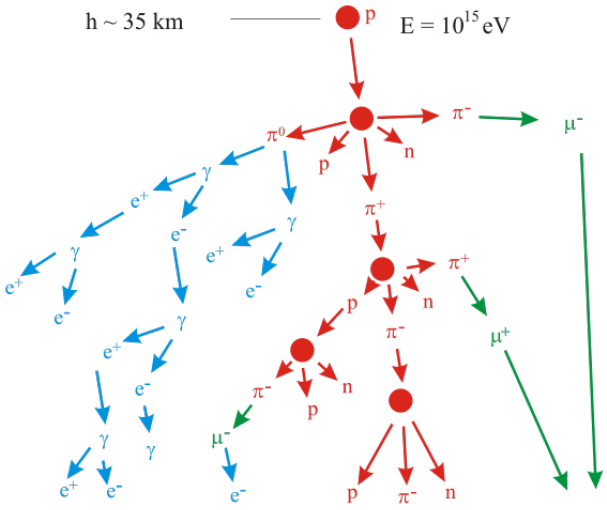

Figure 3: Air shower induced by a cosmic ray (here a proton). Red: hadronic sub-shower. Blue: electromagnetic sub-shower. Green: muons. Decaying pions produce neutrinos. Source: [9].

2 Water cherenkov neutrino detectors

2.1 Atmospheric neutrinos

In order to investigate the above mentioned open questions regarding neutrinos, the detectors ORCA and Super-ORCA need a source of neutrinos. Requirements are a sufficiently large flux in the relevant part of the energy spectrum of one to several GeV, the possibility to allow investigating propagation through matter and the source should be well known in order to make observations of flavour change. Atmospheric neutrinos are such a good source. By observation of "up-going" neutrinos, i.e. neutrinos that reach the detector from through the earth rather then from the atmosphere right above the detector, one can use the earth as a matter probe.

Atmospheric neutrinos are created when high-energy cosmic rays hit the atmosphere and interact there with nuclei, forming a hadronic shower in the process with electromagnetic and hadronic sub-showers, as illustrated in Fig. 3. Protons, neutrons and mesons are produced in the hadronic shower. Decaying mesons can produce muon neutrinos and muons, which again themselves create electron neutrinos when decaying. Both antineutrinos and neutrinos of both flavours are produced due to production of both pions and antipions.

2.2 Detection technique

Because neutrinos are only weakly interacting, a detector naturally requires a large volume of detector material in order to have a sufficiently high event rate to make any statistical observations. Using sea water for (Super-)ORCA allows for a very large detector volume with a high transparency of the material, which is a necessity for a cherenkov detector.

When neutrinos enter the detector medium and interact with nuclei of water molecules charged particles are produced. Both neutrino flavours induce a hadronic shower emanating from where the neutrino interacted with a water molecule. Electron neutrinos additionally create an electron that evolves into a EM shower. Muon neutrinos however produce apart from the original hadronic shower a muon that will eventually decay into a michel electron which produces an EM shower. Fig. 4 shows the visible signature from these events.

For the detection of these charged secondary particles the cherenkov effect is now exploited. The dielectric medium is locally polarized by a passing charged particle and will send out light when the polarization relaxes again. If the particle has sufficient energy so it travels faster then the speed of light in the medium it will stay ahead of the light and the light emission will add up to a cone, like illustrated in Fig. 5. The opening angle of the cone is determined by the velocity of the particle and the detector medium. If one assumes relativistic particles moving at nearly the

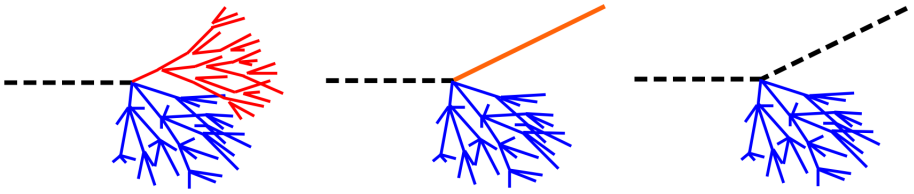

Figure 4: Signatures of neutrino events in detector for electron neutrino (left), muon neutrino (center) and for neutral current interaction (for any flavour) (right). Black: neutrino, blue: hadronic shower, red: EM shower, orange track: muon. Taken from [1].

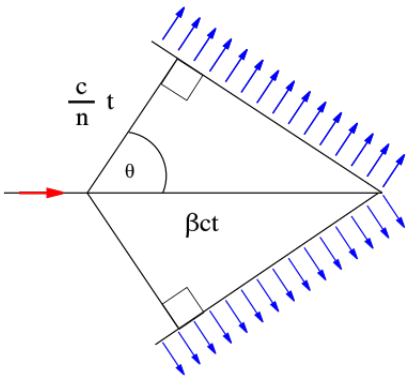

Figure 5: Formation of a cherenkov light cone in two dimensions. The red arrow indicates the direction of the charged particle and the blue arrows the direction of light emission. One can imagine circles forming along the track of the particle that meet up to a united wavefront. Source: [10].

speed of light for water the opening angle becomes $\theta \approx 42^o$ [1]. To detect these light signatures photomultiplier tubes (PMTs) are placed throughout the detector medium, measuring the intensity of the light and the time of arrival.

2.3 KM3NeT/ORCA detector

The ORCA detector of the KM3NeT project[2], currently being built in the Mediterranean sea, is such a neutrino detector that detects atmospheric neutrinos utilizing the cherenkov effect [11]. Its primary goal is to establish the neutrino mass hierarchy with large significance [4].

In Sec. 1.2.1 it was already mentioned that the missing sign of the squared-mass difference can be revealed by observing neutrino propagation in matter. By measuring the incident direction of neutrinos in ORCA the propagation length L from (1) is known and the energy E can also be measured. Discriminating the neutrino flavours in the detector and comparing with models for atmospheric neutrino production one can measure the probability $P_{\alpha\to\beta}$ by gathering large amounts of data. Fig. 6 shows the event rate in the energy zenith angle plane for normal (NH) and inverted hierarchy (IH), i.e. for plus or minus sign of Δm^2_{jk}. One can see regions in the plane with different predictions from NH and IH.

Detector layout From Fig. 1 it is also visible that the desired energy sensitivity of the ORCA detector is at several GeV. The density of light detecting PMTs inside the detector is chosen with respect to this energy range.

To increase overall angular acceptance in the detector the PMTs are arranged in groups on the surface of a sphere. These spheres are called optical module (OM) and contain additional sensors for positioning, read-out electronics and the data and power connection for all its 31 PMTs. The next larger building block are the detection units (DU) that arrange several OMs on a vertical

[2]ORCA/KM3NeT: Oscillation Research with Cosmics in the Abyss / Cubic Kilometre Neutrino Telescope

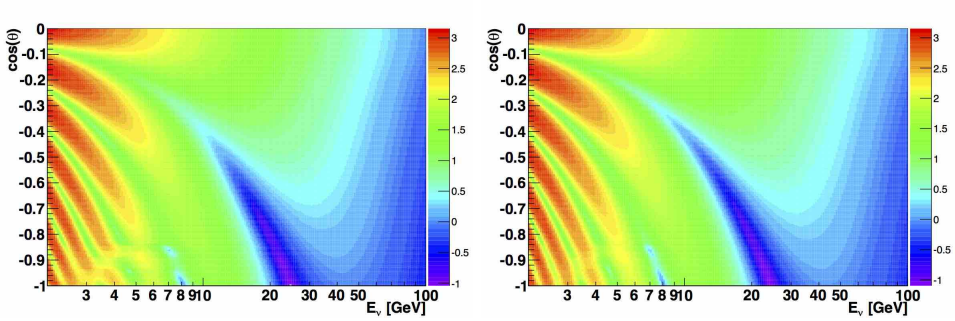

Figure 6: Event rate of muon neutrinos in the energy zenith angle plane for 1 Mton of instrumented detector material. Left: normal hierarchy, right: inverted hierarchy. Taken from [4].

string. For ORCA one string holds 18 OMs and overall the detector has 115 strings arranged in a circular footprint with 106 m radius. The spacing between the OMs is 9 m vertically and between the strings about 20 m horizontally. Fig. 7 shows the schematics of ORCA. Overall the instrumented detector mass is 3.7 Mton. [4]

2.4 Proposed Super-ORCA detector

As the name somewhat suggests, Super-ORCA is a proposed [8] neutrino detector based on ORCA, but with larger PMT density, allowing to measure at even lower energies. This is required to be sensitive to the CP violating phase parameter δ_{CP}, because effects from this parameter come into play at energies below 2 GeV only ([4] p. 11). Similarly to the different event rates for NH and IH in ORCA, for Super-ORCA the CP violating phase will result in a shift in the energy spectrum that is dependant on the value of δ_{CP}.

Detector layout There is no definite layout for Super-ORCA yet and in fact this thesis may contribute to the actual decision regarding the layout. If further studies show that the detection of michel electrons is very important to the operation of Super-ORCA the layout may be adjusted to optimize michel electron detection. However for the purpose of the following analysis a layout has been used that is 10 times denser then ORCA. Instead of 9 m vertical OM distance the simulated Super-ORCA detector uses 3 m vertical inter-OM spacing with 54 OMs per string. The horizontal spacing has been decreased to about 10 m to 12 m and overall 383 strings are spaced out on the same detector footprint (106 m radius).

There are some limits regarding the horizontal spacing between the strings, as there is a risk of entanglement of neighbouring strings due to the strings being non-static structures that are susceptible to sea currents. Deployment also needs some horizontal space. The chosen layout is supposed to meet the desired energy sensitivity while still being realistic.

3 Neutrino reconstruction strategies using michel electrons

A discrimination between anti-/neutrino and between neutrino flavours is necessary due to an opposing effect on the oscillation phase shift [4].

Charge discrimination

- statistics of muons produced in hadronic showers can help discriminate between neutrino and antineutrino. see Fig. 8
- secondary muons invisible due to low energies
- time delay of decay allows seperation from hadronic shower
- more pion+ (pion-) from neutrinos (antineutrinos)

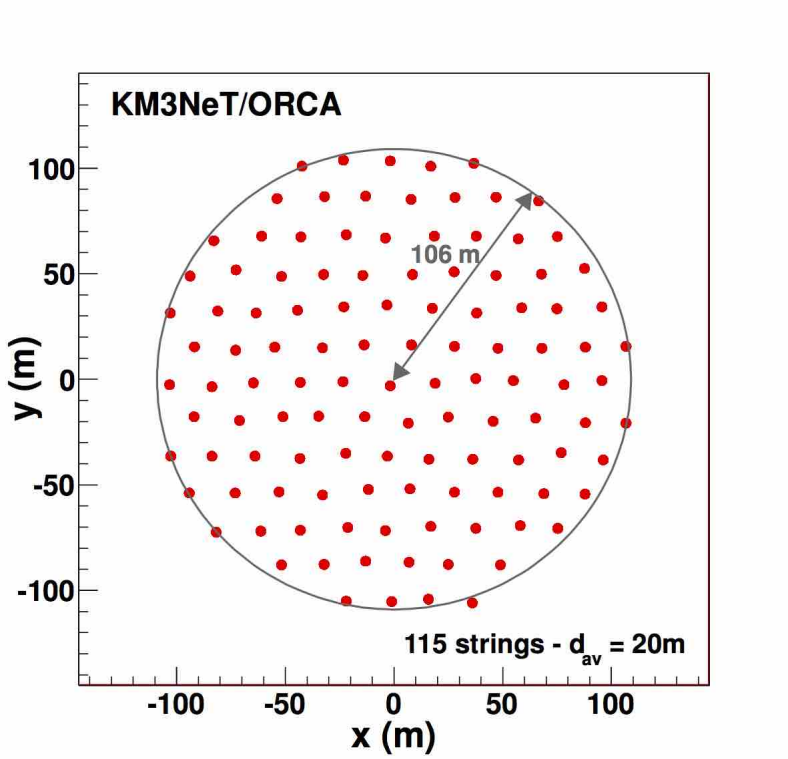

Figure 7: Layout of the ORCA detector. Taken from [4].

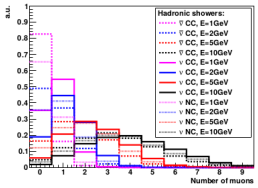

Figure 8: Number of muons produced in hadronic showers. Taken from [1].

4 Development of an michel electron reconstruction algorithm

The main task of this thesis is to give an estimate on the detection efficiency of michel electrons in Super-ORCA. For this purpose a basic reconstruction algorithm for michel electrons needs to be developed. It is only basic because e.g. finding the actual time of decay of the muon will not be implemented but instead it is assumed that a finished algorithm would find this decay time and therefore the actual time from simulated data is used in the estimation. There are also a number of occasions where further investigation opportunities have not been seized due to time constraints. They will be summarized in Sec. 6.

In the following data from monte carlo simulations is used that has been computed using the detector layout described in Sec. 2.4.

Definitions and assumptions The following nomenclature is used throughout this section:

- **event**: Single muon decay that produces single michel electron that induces an EM shower which can be detected by cherenkov radiation.
- **signal hit**: Single PMT detecting cherenkov light photons from michel electron (or its EM shower).
- **noise hit**: Single PMT detecting photons that are from background noise and not related to a michel electron.
- **vertex**: The location of the muon decay which is assumed to be the very same location as the origin of cherenkov light. It is assumed that the vertex location is known.[3]

All signal hits in the following are signal hits with applied smearing. Data from the originally non-smeared signal simulation has been used to find the smeared signal hits from the simulation producing smeared signal/noise mixture. There is a small possibility that noise hits are not recognized correctly by this separation process or that signal hits end up as noise hits.

For all of the following events with less then 3 signal hits have been discarded. This was done originally to suppress signal hits originating from other charged particles then michel electrons, e.g. from protons, neutrons or pions (see Fig. 9). These can be created by interactions between the muon and nuclei. However due to the charge of the nucleus this is only the case for μ^- and not for μ^+. Because of this only events involving antimuons decaying into "michel positrons" are analyzed and the original reason for discarding events with less then 3 signal hits is nt valid anymore. However including these events will probably not lead to a very different result, as events with 2 or only 1 signal hit are rated poorly by the reconstruction algorithm anyways (see Sec. 4.3.2).

4.1 Background noise[4]

Differentiating between noise and signal hits is the goal of this reconstruction algorithm. Basically three sources of background noise can be distinguished: The unavoidable dark count rate, background from radioactive decays in the detector medium and light contamination from bioluminescence. The dark count rate comes from thermal noise and radioactive decays inside the material of the PMTs themselves and is entirely isotropic. It is also not correlated and can therefore be suppressed quite easily. Organisms in the deep sea capable of bioluminescence use chemical reactions to emit light which is visible as an isotropic noise level, but can also produce bright bursts of light. These influence the detector significantly, however the light bursts are on larger time scales (seconds) then neutrino events (micro seconds).

Radioactive decay inside the sea water, mainly from potassium 40 (K-40), also contributes isotropically to the noise level. However, radioactive decays are also a correlated source of noise which can be hard to distinguish from signal hits. The β-decay of K-40 produces an electron that

[3] For primary muons, i.e. the high-energetic muon from a muon neutrino interaction (outside of the hadronic shower), this location can be found by determining the end of the muon track.

[4] closely follows [1]

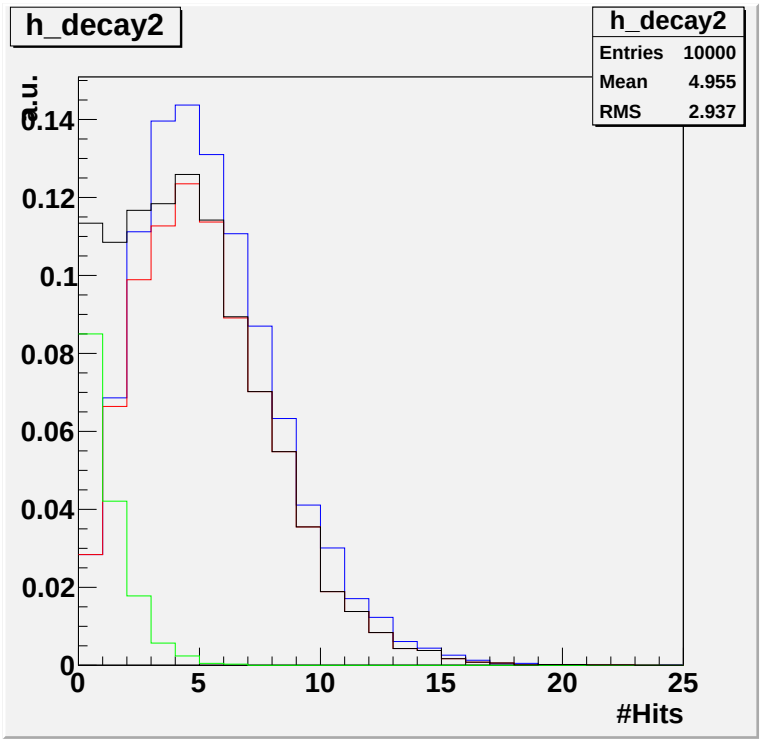

Figure 9: Frequency distribution of signal hits for simulated μ^+ and μ^- events. Blue: all hits from μ^+ event, black: all hits from μ^- events. Red (green) curve show origin of cherenkov light for μ^- events from michel electrons (other particles)

has a large enough energy to form an EM shower and emit cherenkov light. If a K-40 decays in the vicinity of the vertex its light emission cannot be easily distinguished from those of an michel electron.

The isotropic background rate of radioactive decays contributes about 100 Hz per cm^2 of PMT surface area. A quick estimation[5] shows that within the interesting timespan of 5 μs after a neutrino event about 13,000 noise hits are registered in the whole detector. This is opposed to only a few signal hits per michel electron and demonstrates that an effective noise suppression is vital.

4.2 First stage: per-hit criteria

As a first step in separating signal from noise each hit will be processed individually without factoring in any correlation between hits. In this process each hit will be assigned a probability that gives the "signalness" of the hit. To combine several separately calculated hit probabilities we will form the product of these. Using the (normalized) sum of probabilities has the disadvantage that a large probability could compensate a probability of zero, which is not desired.

Three criteria will be investigated in the following. The total probability for a hit to be a signal hit is then:

$$P_{tot} = P_{aa} * P_{tres} * P_{abs} \tag{2}$$

4.2.1 Angular acceptance of PMTs

The first criterion is the angular acceptance of a PMT. Depending on the incident angle of the photons a PMT has a different sensitivity, so if the vertex is located in the periphery of the field

[5]The diameter of the light collection area of the PMTs used in the detector is about 7.2 cm. The whole detector uses a total amount of 641,142 PMTs.

of view of the PMT or even outside its field of view it is less probable that a hit recorded by this PMT is a signal hit.

The field of view of a PMT is slightly larger then 180^o due to the light collector being convex. Additionally the optical structures of the OMs are constructed such that light collection towards the PMTs is maximized. However even outside of an angle of about 200^o light collection possible due to backscattering in the medium: it is possible that photons originating opposite to the viewing direction of a PMT get past the PMT into its field of view, get scattered in the medium and finally hit the PMT. Within the field of view the sensitivity of a PMT is highest if the indicent angle is 0^o, i.e. parallel to the PMT direction, and lowest if the photons arrive from the very side.

This angular acceptance is modelled by the cosine of the incident angle θ that is adjusted such that minimum acceptance is at $\cos(\theta) = -0.1$, i.e. at an angle slightly larger then 90^o.

The uncertainty of the position of the vertex is most probably large and for Super-ORCA the distances between OMs are very small so that a PMT that is close to but facing away from the vertex could actually (within the error margin of the position) be facing the vertex perfectly. To accommodate for this fact a distance-dependant adjustment is introduced that increases the angular acceptance interval for PMTs close to the vertex.

For each hit the angle between facing direction of PMT and direction towards vertex can be calculated. This algorithm will accept this angle and assign a probability P_{aa} for this hit to be a signal hit due to angular acceptance.

4.2.2 Time residual

The time residual is the difference between the arrival time of a photon at a PMT and the expected arrival time due to propagation speed. It is zero if the photon propagates with the expected velocity and without scattering, so if the photon takes the shortest route:

$$t_{res} = t_{arrival} - t_{emission} - \frac{d}{c_{water}} \tag{3}$$

where c_{water} is the speed of light in sea water and d is the distance between PMT and vertex. The time of emission is assumed to be known.

In comparison to the angular acceptance the time residual depends on two parameters $t_{arrival}$ and d. This makes it difficult to create a model in form of an equation. Therefore the statistics of a large amount of simulated signal hits will be used: for about two million simulated signal hits the time residual is calculated and added to a 2-dimensional histogram with time residual and distance to vertex as axes. The histogram is normalized to be 1 at a time residual of 0 and with that holds the frequency distribution in the time residual-distance plane. Fig. 10 shows a projection of this 2-dimensional histogram.

This histogram can be used as a look-up table: for a hit the time residual is calculated and this time residual together with the distance determine a probability P_{tres} by interpolating in the histogram for the specific values of time residual and distance. This is more precise then just using the histogram bins that are closest to the specific values.

After several tens of nanoseconds in the time residual there is a sharp decline in probability. In order to increase the performance of the algorithm the probability will be set to 0 (or a very small value) if $t_{res} > 10\ ns$.

4.2.3 Absorption in sea water

During their propagation in the detector medium the cherenkov photons get absorbed by interacting with matter. The detection probability of light decreases exponentially with the distance from the vertex. The absorption length is wavelength-specific and apart from absorption there is also a scattering effect. By taking the scattering effect into account and averaging over the wavelength one can eventually assign a typical average absorption length of $\lambda = 35\ m$ [1].

The signal probability due to light absorption is therefore just an exponential decay. With the distance d from the vertex the probability is given as:

$$P_{abs} = \exp\left(-d/\lambda\right) \tag{4}$$

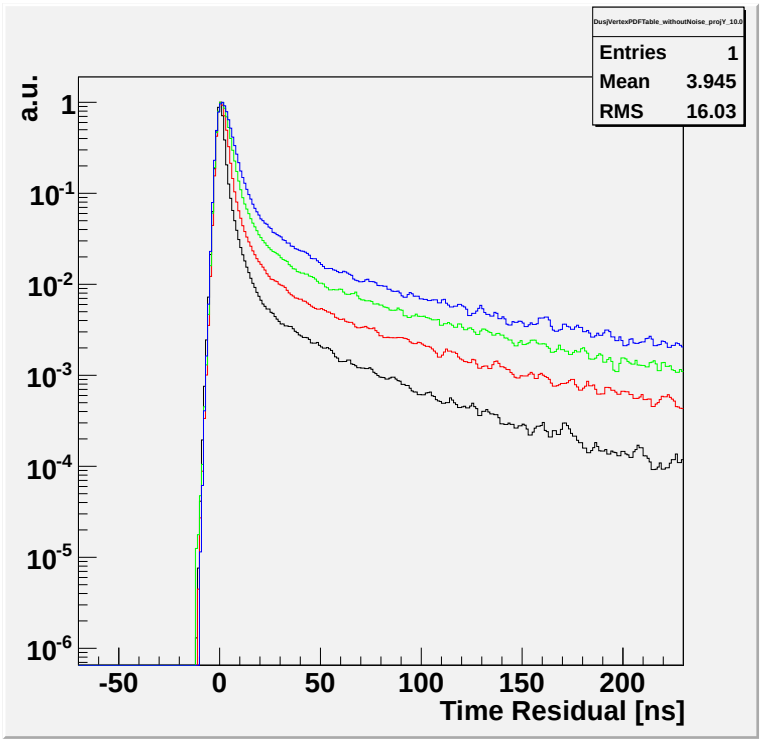

Figure 10: Frequency distribution of time residual for signal hits. Black, red, green and blue lines are cuts through distance-time residual plane for distances of 10 m, 30 m, 50 m and 70 m respectively.

4.3 Second stage: per-event criteria

Signal probabilities for individual hits are a good way to determine signal hits, however they do not suppress noise hits actively. For each event we expect more then one signal hit most of the time (see 9), therefore we can develop selection criteria that take into account correlation between several hits. To determine the hit correlation the best hits (largest P_{tot}) per event are selected and the correlation between those is calculated.

4.3.1 Pairwise hit correlation

The correlation between a number of hits can be reduced to a number of pairwise correlations between all hits. Therefore only pairwise hit correlation, i.e. correlation between only two hits at a time, is investigated in the following.

If two hits are correlated they are said to be "cone-like": the position of the hits are on the surface of the cherenkov light cone originating at the vertex. The statistics of the correlation are investigated by looking at the distance between the two hits and the distances between each hit and the vertex, which are three parameters. A frequency distribution as a 3-dimensional histogram is created by using simulated signal hits. Fig. 11 shows one example. A periodicity is clearly visible that comes from the detector layout. Recording a frequency distribution using noise hits which are isotropic and will therefore show the detector geometry and diving the above example by this eliminates the periodic structures. The data is then normalized and rebinned to smooth out random fluctuations, which gives Fig. 12. This is then used as look-up table to get the probability for hit correlation between two hits.

For more then two hits the correlation probability P_{corr} is defined as the product of all pairwise correlation probabilities (e.g. hits 1, 2 and 3: product of values for "1 and 2", "2 and 3" and "1 and 3").

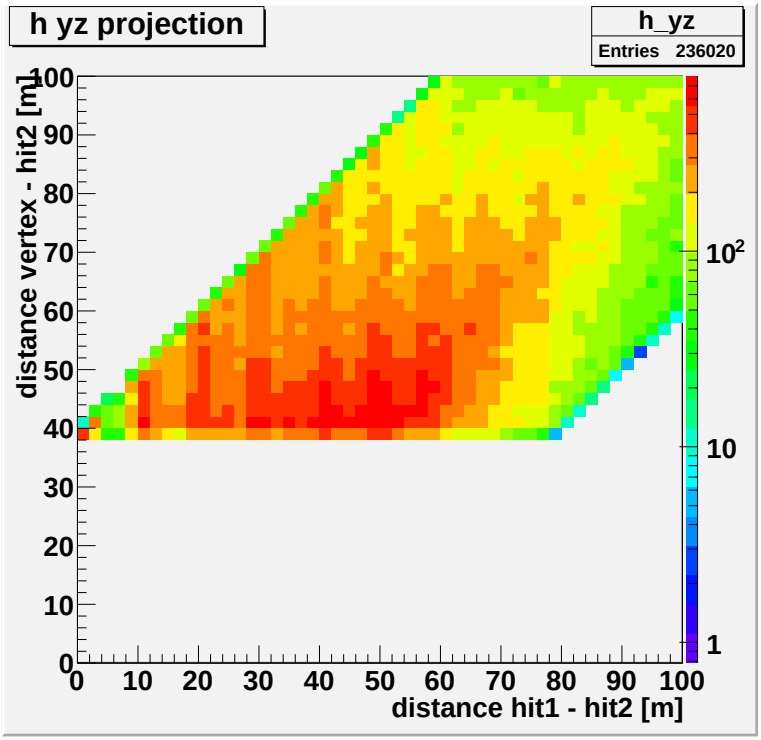

Figure 11: Frequency distribution of hit correlationl for signal hits. Cut through a 3-dimensional histogram at vertex-hit1 distance of 40 m.

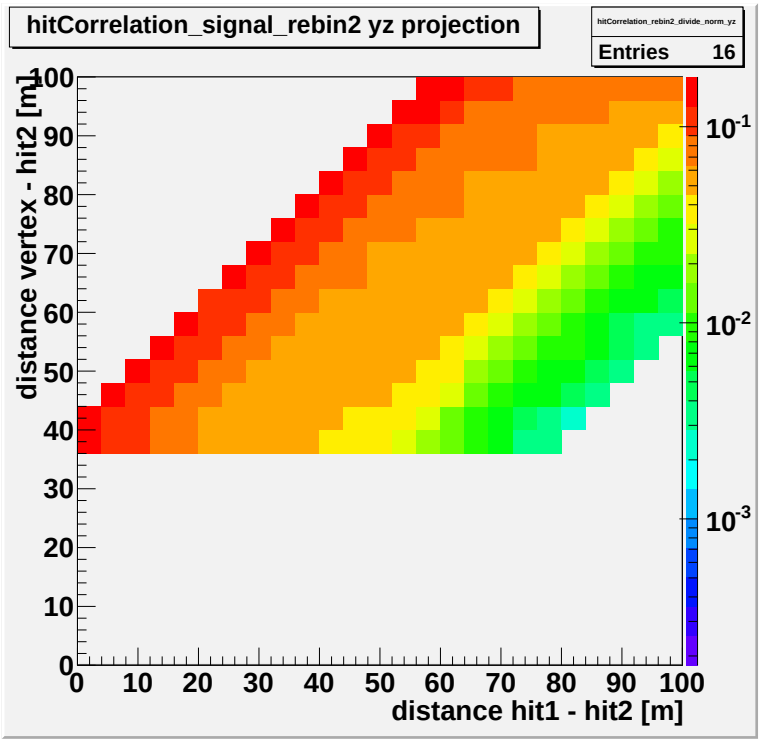

Figure 12: Frequency distribution of hit correlation for signal hits. Cut through a 3-dimensional histogram at vertex-hit1 distance of 40 m. Divided by noise data and rebinned.

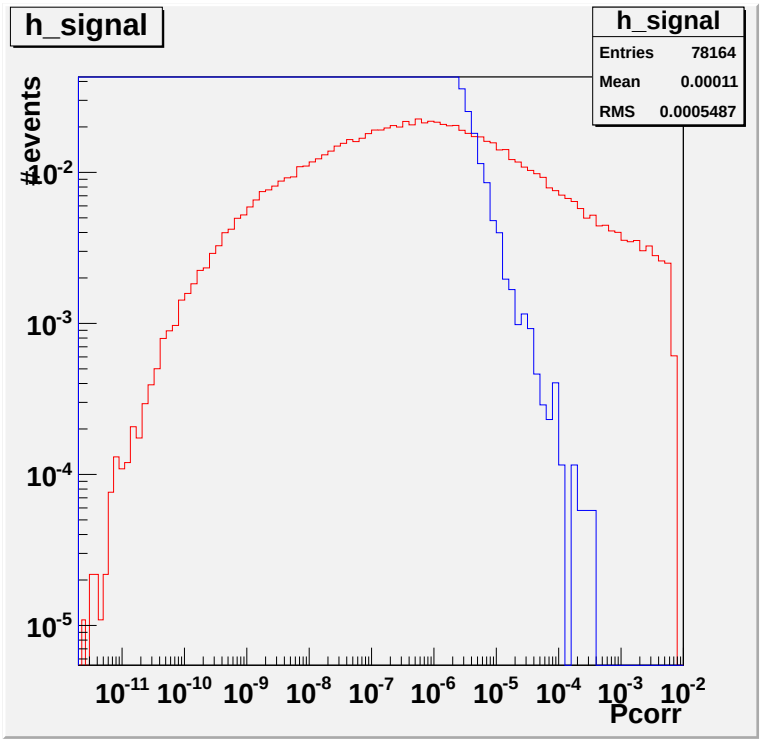

Figure 13: Red: Signal/noise mix normalized to 1, blue: noise normalized to 1000. For $N = 6$, $M = 3$.

4.3.2 Final hit selection

The eventual goal is to find the best candidates for signal hits of an event and to assign the event a probability for it to be an actual signal event. Calculating the correlation probability makes sense only for best hits of an event (regarding per-hit criteria): we expect all signal hits to be among the best hits plus some noise. Hit correlation will then remove the signal-like noise hits because they do not fit together with the real signal hits. K-40 decays are still posing a risk of miss-identification as they are correlated. This is a point that may be worth further investigation.

In order to find a group of the best correlated hits from the individually best hits: selecting best N hits and of those calculate correlation between M hits ($M < N$) for all possible combinations. The product of hit correlation probability and single hit probabilities P_{tot} gives value that is maximal for group of hits made of signal hits.

Groups of $M = 3$, 4 and 5 hits are investigated with $N = 6, 8, 10$ respectively. This selection is performed for large sample size of signal/noise mix (of which the majority will be signal) and only-noise hits. The frequency distribution can be seen in Fig. 13.

5 Estimation of detection efficiency

Above distribution of signalness probability for both signal/noise mix and noise can be used to estimate efficiency of detector for signal/noise discrimination. The goal is a efficiency vs purity plot, i.e. the fraction of events that can be identified as signal with a specific (un)certainty.

5.1 Time dependency

We have assumed to know time of muon decay before, however it would need to be determined by time scanning: assume decay time at time t and let t run from 100 ns to 5000 ns with 0 being neutrino event time. Omit the first 100 ns (about 5 percent of events) because of neutrino event lighting up the detector. Beyond 5000 ns only 9 percent of events. The signalness would need to

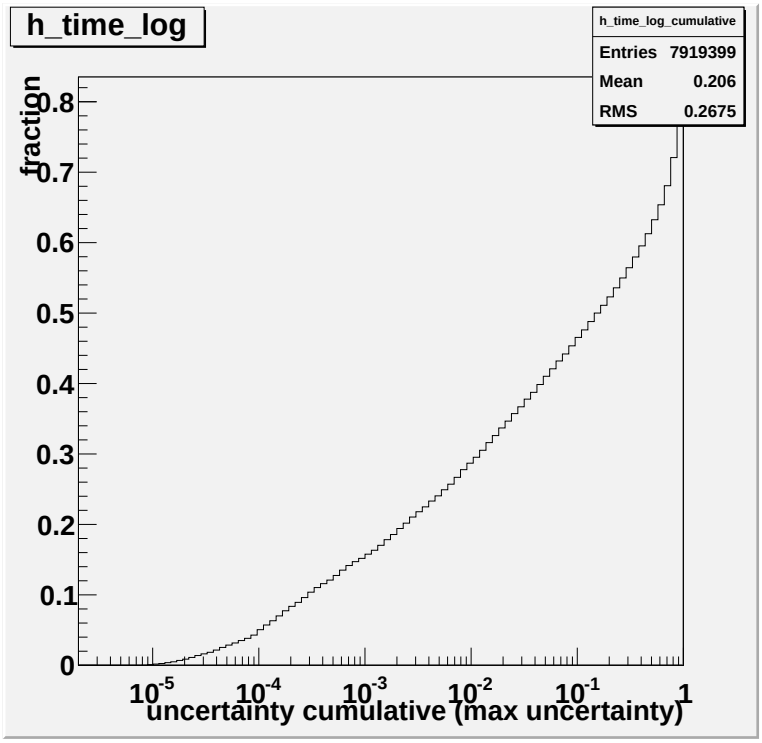

Figure 14: fraction of events that are identifiable as signal events for desired maximum uncertainty (cumulative, i.e. "with this or less uncertainty" = "with this or more one minus certainty"). for M =3, $N = 6$ scenario

be calculated for all assumed times and by that the correct time would be found. This is not done here, as we only want to estimate the efficiency of a possible reconstruction algorithm.

The probability for muon decay is exponentially decreasing with muon half life of 2200 ns: $\exp\left(-\frac{t}{2200\ ns}\right)$. Signal distribution is normalized with this exponential function to accommodate lower probability for muon to decay at larger times.

5.2 Results

From the signalness distribution of signal and noise (13) we can extract the fraction of signal events and the certainty: for each bin the value of signal curve is the fraction of events that can be identified as signal events with a specific certainty. The certainty of identification is $cert = \frac{signal}{signal+noise}$ for each bin.

This process is done for $N = 10, 8, 6$, however hardly any difference is visible (Fig. 14, 15, 16). These are plotted cumulatively so one can see easily how many events can be identified as signal with which maximum uncertainty (or minimum one minus certainty).

The results are: With a 90 / 99 / 99.9 percent security we can identify 50 / 30 / 20 percent of events as signal events.

6 Outlook

There are a number of points that are interesting for further investigations:

- further noise suppression for correlated noise from K-40 decay
- investigate μ_- as well because this thesis only investigated μ_+. difference: μ_- interacts with matter, therefore we have to lower the estimate

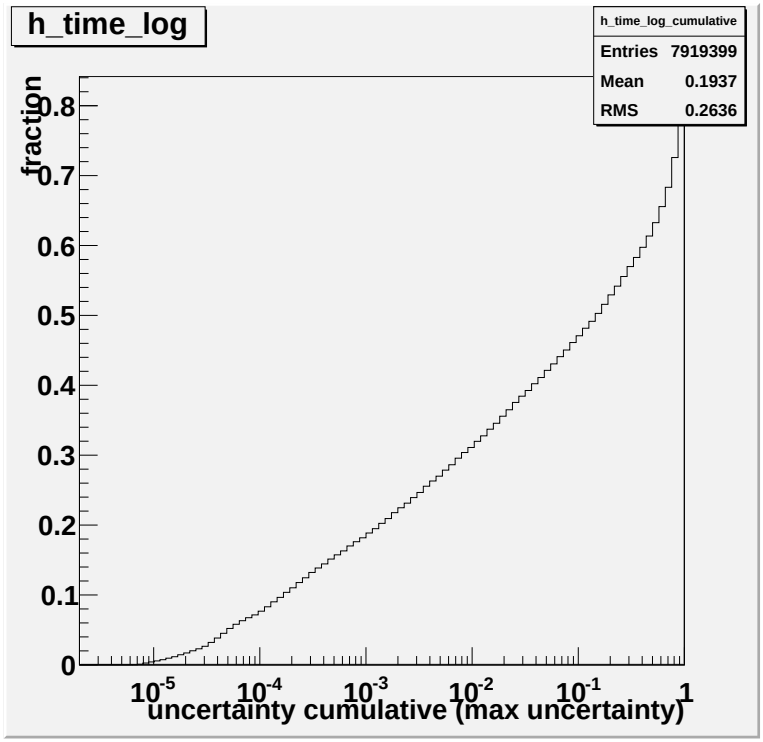

Figure 15: fraction of events that are identifiable as signal events for desired maximum uncertainty (cumulative, i.e. "with this or less uncertainy" = "with this or more one minus certainty"). for M =4, $N = 8$ scenario

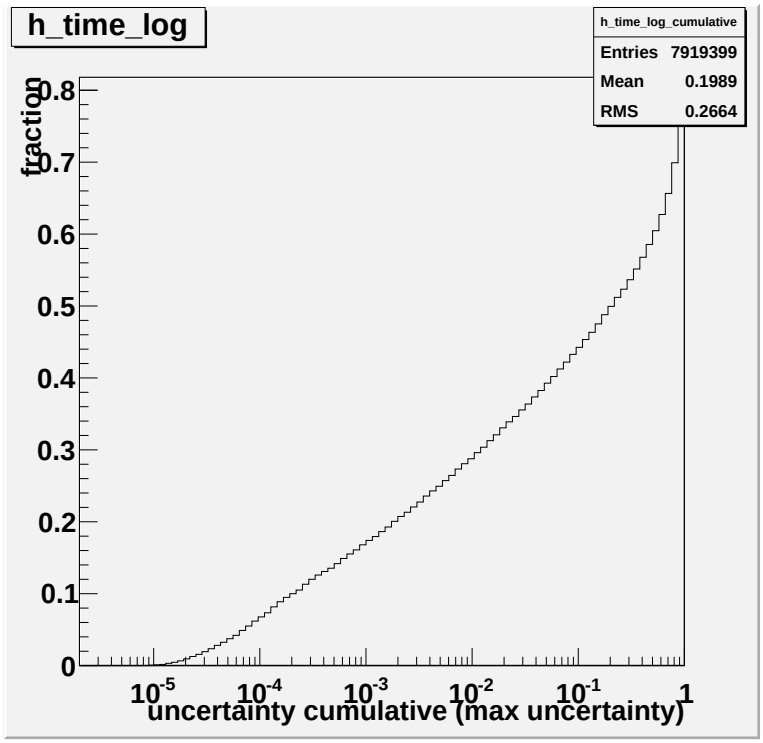

Figure 16: fraction of events that are identifiable as signal events for desired maximum uncertainty (cumulative, i.e. "with this or less uncertainy" = "with this or more one minus certainty"). for M =5, $N = 10$ scenario

- interaction of μ_- with matter in comparison to non-interaction of μ_+ can be used to discriminate between anti-/neutrino directly
- possibly a better angular acceptance algorithm

References

[1] Jannik Hofestädt, *Measuring the neutrino mass hierarchy with the future KM3NeT/ORCA detector*, Ph.D. Thesis, University of Erlangen-Nürnberg, 2017.

[2] Fukuda, Y. and others, *Evidence for oscillation of atmospheric neutrinos*, Physical Review Letters **81**, 1562 (1998), [hep-ex/9807003].

[3] R. Slansky et al., *The oscillating neutrino: An introduction to neutrino masses and mixings*, Los Alamos Sci. **25**, 28 (1997).

[4] KM3NeT Collaboration, *Letter of Intent for ARCA and ORCA*, 2016, [arXiv:1601.07459v2[astro-ph.IM]].

[5] *Hyper-Kamiokande*, Website `http://www.hyper-k.org/en/physics/img/hierarchy_spheres_english.png`.

[6] Wu, C. S.; Ambler, E.; Hayward, R. W.; Hoppes, D. D.; Hudson, R. P., *Experimental Test of Parity Conservation in Beta Decay*, Physical Review **105** (4): 1413–1415, 1957.

[7] J. H. Christenson; J. W. Cronin; V. L. Fitch and R. Turlay, *Evidence for the* 2π *Decay of the* K_2^0 *Meson System*, Physical Review Letters **13**: 138, 1964.

[8] T. Eberl, *Nachweis von Tauneutrinos mit ORCA und Bestimmung der leptonischen CP-Phase mit Super-ORCA*, proposal for research grant, 2016.

[9] *Wikimedia*, Website `https://upload.wikimedia.org/wikipedia/commons/2/2c/AirShower.svg`.

[10] *Wikimedia*, Website `https://upload.wikimedia.org/wikipedia/commons/6/6b/Cherenkov.svg`.

[11] *KM3NeT*, Website `http://www.km3net.org/`.

Erklärung

Hiermit erkläre ich, dass die vorliegende Bachelorarbeit von mir eigenhändig verfasst wurde und ich keine Hilfsmittel und Quellen als die angegebenen verwendet habe.

Sebastian Schindler Erlangen, 28.07.2017